Staged Diafiltration Cascades Provide Opportunities to Execute Highly Selective Separations

Cara P. Kilmartin[#], Jonathan Aubuchon Ouimet[#], Alexander W. Dowling, and William A. Phillip[*]

Department of Chemical and Biomolecular Engineering, University of Notre Dame, Notre Dame, Indiana 46556, United States

* To whom correspondence should be addressed: wphillip@nd.edu

[#]Cara P. Kilmartin and Jonathan Aubuchon Ouimet contributed equally to this work.

Abstract

Improved solute selectivity, an issue commonly approached through the development of advanced membrane materials, can be achieved through staged diafiltration processes. A mathematical model that describes the solute concentration profile within a single diafiltration module is developed and experimentally-validated. For this module, where the diafiltrate is introduced uniformly over its length, a critical diafiltrate flux that results in the retentate concentration remaining constant during operations is identified. The model is then extended to examine two configurations of multistage diafiltration cascades: stripping sections and rectifying sections. The two configurations differ based on the connectivity between stages. Namely, stripping sections connect multiple modules by utilizing the retentate from one stage as the feed to the subsequent stage while the permeate is repurposed as the diafiltrate. In contrast, rectifying sections utilize the permeate from one stage as the feed to the subsequent stage and the retentate becomes the diafiltrate. For cascades that operate with a constant diafiltrate to feed flow ratio for all stages, the analysis demonstrates that stripping sections can reduce the diafiltrate consumed when separating low molar mass impurities from larger, impermeable molecules. On the other hand, cascades in a rectifying section configuration can improve the separation of two solutes with finite sieving coefficients between 0 and 1. Finally, asymmetric cascades, i.e., systems in which each stage has a unique diafiltrate to feed flow ratio, are shown to be capable of improving the recovery and purity of solutes in effluent streams relative to system that operate at constant a diafiltrate to feed ratio. As a whole, the study highlights that the continued advancement of membrane separations will rely equally on thoughtful module and process design as well as the development of new materials.

1. Introduction

The development of more selective separation processes is necessary to meet society's growing materials and energy demands sustainably.[1–3] For example, in the area of water treatment, driven by their finite amounts and negative impacts on human health and the environment, there is an emerging trend to view the nutrients (e.g., nitrogen- and phosphorous-containing species) dissolved in wastewater as a valuable resource that can be recovered.[4–6] Similarly, the projected increase in consumer electronics and electrical vehicles will increase the demand for critical, raw resources (e.g. lithium, cobalt, nickel, rare earth elements). Increased recycling of electronic components[7] and batteries[8], enabled by new separation techniques[9] can begin closing the loop to create a circular economy. In some instances, recycled materials have the potential to be acquired at lower economic and energetic costs then their mined counterparts.[10,11]Additionally, there is an environmental incentive to forgo the harsh chemicals and solvents traditionally used in the purification of raw and recycled materials.[8] Biomanufacturing has its own needs for advanced separation processes. With increasingly stringent regulations, a significant amount of research has investigated the development of reliable and continuous processing technologies.[12–15] In order to meet these wide-ranging demands across several industries, many studies have been aimed at the creation of more selective membrane materials.[16–23]

While more selective membranes based on advanced materials can help to improve separation processes,[24,25] translating materials advances to industrial scales will require the intersection of materials, device, and systems design[25]. For instance, the transition toward continuous biomanufacturing processes demonstrates how novel device and systems designs are needed to advance separations science. Here, motivated by the reduced costs, improved quality control, and greater flexibility that are associated with single-pass unit operations, there is an

emerging interest in the design and implementation of continuous countercurrent diafiltration cascades.[26] Single-stage diafiltration processes are used widely in the production of biopharmaceutical products. However, in addition to their intermittent, batch operation, these designs have high pumping costs that result from the need to recirculate the retentate many times on the upstream side of the membrane. Rucker-Pezzini *et al*. demonstrated that a fully continuous diafiltration process was capable of achieving 99.75% buffer exchange in a single pass for the purification of monoclonal antibodies.[12] However, because fresh diafiltrate solution was introduced at the beginning of each stage, the total volume of diafiltrate needed was greater than a traditional batch diafiltration process. Recently, Nambiar *et al*. demonstrated a countercurrent diafiltration process, where the permeate from one stage was repurposed as the diafiltrate for the next stage, could be utilized to reduce the volume of diafiltrate required while retaining a single-pass design that decreased pumping costs.[27] While the two-stage design considered didn't achieve the desired level of buffer exchange, model calculations informed the addition of a third stage, which resulted in a process that achieved high purity (i.e., 99.9% buffer exchange).[28] The opportunities for staged diafiltration are not restricted to biopharmaceutical formulations. For example, Siew *et al*. demonstrated that multistage diafiltration designs are also capable of targeting the removal of impurities in the context of organic solvent nanofiltration.[29]

The literature on staged diafiltration focuses primarily on buffer exchange/formulation processes whereby small impurities are removed from solutes that are rejected by the membrane. Given the emerging need for solute-selective separations, there may be opportunities to utilize diafiltration for the fractionation of solutes with comparable molecular characteristics. In this regard, Barker and Hill demonstrated that a series of modules, equipped with membranes that possessed different molecular weight cutoffs, could be used to separate similarly-sized dextran

molecules.[30] In addition to advances at the systems-scale, there are opportunities for improved designs at the device-scale. As one example, Tan *et al*. reduced the complexity of a diafiltration system by 3D printing a single-stage module that systematically dosed the diafiltrate directly into the retentate.[31] In this design, the length of the module determined the achievable purity.[31]

Given this context, the objective of this study is to consider the design and operation of staged diafiltration cascades for solute-selective separations. A mathematical model is developed to describe the performance of a single stage in which the diafiltrate is dosed into the retentate continuously over the length of the module. Experiments utilizing a modified dead-end stirred cell are executed to test the model and examine the operating regimes of this design. Subsequently, the model is extended to examine the design of multistage cascades. The configuration of the cascades, which is controlled through the connectivity between stages, is shown to determine the types of separations that stripping and rectifying section configurations are well-suited to execute. The discussion also highlights how novel module designs can be leveraged to further enhance the performance of diafiltration cascades for executing highly-selective separations.

2. Theory

2.1 Single-stage Analysis.

Assuming a dilute solution, governing equations for the system presented in Figure 1A can be derived from mass balances on the solvent and solute, Equations 1 and 2, respectively.

$$\frac{dv^0}{dz} = J_D a_m - J_w a_m \qquad 1$$

$$\frac{d(c_1 v^0)}{dz} = J_D c_D a_m - J_s a_m \qquad 2$$

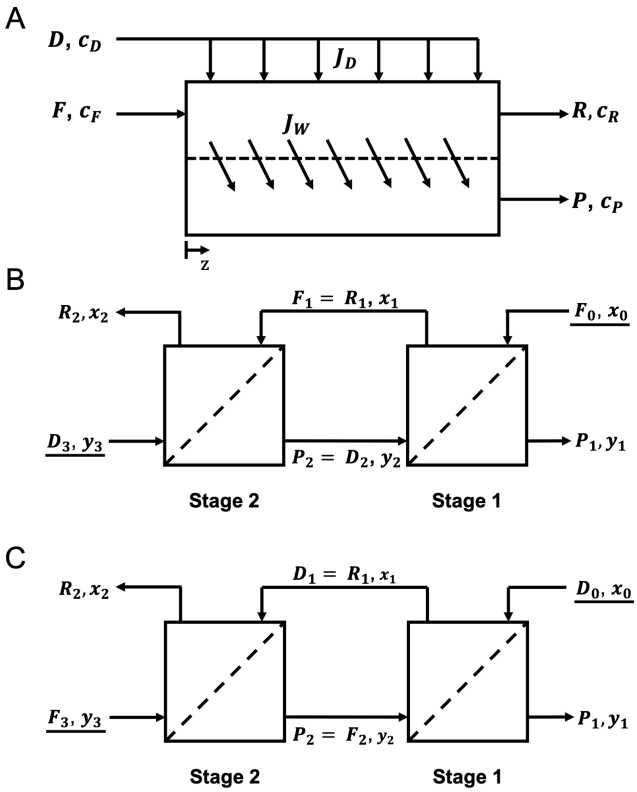

Figure 1. A single-stage diafiltration module and two multistage diafiltration cascade configurations are shown schematically. (**A**) Within the single-stage system, the feed stream enters at a flow rate, F, and concentration, c_F. A diafiltrate flow, D, with concentration, c_D, is dosed uniformly, as the flux J_D, on the upstream area of the membrane. The volumetric flux across the membrane, J_W, is driven by an applied pressure. The permeate leaves the crossflow device at a flow rate, P, and concentration, c_P. The solute and solvent that are retained by the membrane leave through the retentate stream, R, with concentration, c_R. Panels (**B**) and (**C**) present schematics for two possible configurations of a two-stage diafiltration system, a stripping and a rectifying section, respectively. In the crossflow designs, the streams have dynamic definitions that change when moving between stages. Thus, instead of defining the concentrations in terms of the permeate, retentate, feed, or diafiltrate, the molar concentrations in the overflow are denoted by x_n and the molar concentrations in the underflow are denoted by y_n, where n indicates the stage from which the flow originated from. (**B**) For the stripping section, an initial feed with flow rate F_0 and concentration x_0 is introduced to stage 1. The initial diafiltrate enters the system at stage 2 with flow rate D_3 and concentration y_3. The permeate from stage 2, P_2, enters stage 1 as the diafiltrate, D_2, at concentration y_2. The permeate solution from stage 1, P_1, is collected as a product steam. The retentate flow from stage 1, R_1, enters stage 2 as the feed flow F_1. The final retentate stream R_2 is collected as a product at x_2. (**C**) The rectifying section introduces the initial feed flow, F_3, into stage 2 at concentration y_3 and the initial diafiltrate flow, D_0, into stage 1 at concentration x_0. The permeate, P_2, exits stage 2 and is fed into stage 1 at a concentration y_2. Similarly, the retentate, R_1, exits stage 1 and becomes the diafiltrate for stage 2, D_1, both with concentration x_1. The locations of the final retentate and permeate streams remain the same in both configurations.

This model uses a constant volumetric flow rate D, which is distributed uniformly along the

membrane module, for the diafiltrate such that it can be represented by the term $J_D a_m A_c \Delta z$. J_D is the volumetric flux of the diafiltrate, a_m is the membrane area per module volume, A_c is the cross-sectional area of the module, and Δz is the change in the length down the module. In a similar manner, the volumetric flow rate of the solvent and the molar flow rate of the solute through the membrane were represented by the terms $J_w a_m A_c \Delta z$ and $J_s a_m A_c \Delta z$, respectively. J_w is the volumetric flux of solvent and J_s is the molar flux of solute. Integrating Equation 1 allows the solution velocity, v^0, to be determined, Equation 3.

$$v^0 = (J_D - J_w) a_m z + v_f^0 \qquad 3$$

The initial feed velocity, v_f^0, can be calculated from F/A_c where F is the volumetric flow rate of the feed.

Rearranging the solute balance using the product rule and expressing the solute flux as $J_s = J_w S c_1$ results in Equation 4.

$$0 = -c_1 \frac{dv^o}{dz} - v^o \frac{dc_1}{dz} + J_D c_D a_m - J_w a_m S c_1 \qquad 4$$

Here, the sieving coefficient, S, which quantifies the ability of the solute to pass through the membrane, is introduced to relate the solute concentration in the permeate to its local upstream concentration, c_1. Within the current framework, S is the actual sieving coefficient, which depends only on the membrane characteristics. The observed sieving coefficient, which accounts for the effects of concentration polarization, can be related to the actual sieving coefficient using known relationships.[32] These relationships, however, depend on mass transfer coefficients that are module specific. Consequently, this correction for concentration polarization is left for future consideration. Substituting Equation 1 and Equation 3 into Equation 4 results in Equation 5, which can be solved using the method of integration factors.

$$\frac{dc_1}{dz} + \frac{(J_D a_m - J_w a_m (1 - S))}{(J_D a_m - J_w a_m)z + v_f^0} c_1 = \frac{J_D a_m c_D}{(J_D a_m - J_w a_m)z + v_f^0} \quad 5$$

Simplifying through substitutions provides an equation for the evolution of the upstream solute concentration profile.

$$\frac{c_R}{c_F} = \frac{\delta G}{S + \delta - 1} + \left(1 - \frac{\delta G}{S + \delta - 1}\right)(V(\delta - 1) + 1)^{\frac{1-\delta-S}{\delta-1}} \quad 6$$

$$\delta = \frac{J_D}{J_w} \ , \ G = \frac{c_D}{c_F} \ , \ V = \frac{J_w a_m z}{v_f^0}$$

In Equation 6, *G* represents the diafiltrate concentration normalized by the feed concentration. The feed volumes, *V*, represents the volume of solution permeated across the membrane relative to the initial feed volume, and δ is the ratio of the diafiltrate flux to the solvent flux. The product of δ and *V* is equal to the diavolumes.

Equation 6 generates finite solutions in cases where $\delta \neq 1$. In the limit that $\delta = 1$, $J_w = J_D$ and the solvent velocity is constant, $\frac{dv^0}{dz} = 0$. As such, Equation 4 reduces and can be solved using an integration factor to give Equation 7.

$$\frac{c_R}{c_F} = \frac{G}{S}(1 - e^{-VS}) + e^{-VS} \quad 7$$

Equation 7 allows for the direct comparison of model predictions to experimental results as the experimental setup operates at $\delta = 1$.

2.2 Multistage System: Stripping Section.

Multiple modules can be interconnected to generate staged cascades. Figure 1B shows a stripping section where the retentate from one stage becomes the feed to the subsequent stage. The permeate is then utilized as the diafiltrate. To analyze the performance of this staged design, the volumetric flows within the cascade are expressed in terms of the solvent recovery for each stage,

$Y_{w,n}$. The solvent recovery represents the amount of solution permeated across the membrane relative to the amount of solution flowing into a stage via the feed and diafiltrate streams.

$$Y_{w,n}^{S} = \frac{P_n}{F_{n-1} + D_{n+1}} \quad 8$$

Assuming that the inlet flow rates D_3 and F_0 are known, the remaining flow rates are derived from overall mass balances surrounding each stage.

$$R_1 = F_1 = \frac{(1 - Y_{w,1})(F_0 + Y_{w,2}D_3)}{(1 - Y_{w,2} + Y_{w,1}Y_{w,2})} \quad 9$$

$$P_1 = Y_{w,1}\left(\frac{F_0 + Y_{w,2}D_3}{1 - Y_{w,2} + Y_{w,1}Y_{w,2}}\right) \quad 10$$

$$R_2 = \frac{(1 - Y_{w,2})(D_3 + (1 - Y_{w,1})F_0)}{1 - Y_{w,2} + Y_{w,1}Y_{w,2}} \quad 11$$

$$P_2 = D_2 = Y_{w,2}\left(\frac{(1 - Y_{w,1})F_0 + D_3}{1 - Y_{w,2} + Y_{w,1}Y_{w,2}}\right) \quad 12$$

Furthermore, using the inlet concentrations x_0 and y_3 as known conditions. Species mass balances and a version of Equation 6 written for each stage results in the following linear system of equations (Supporting Information).

$$\begin{bmatrix} F_1 & 0 & P_1 & -P_2 \\ -F_1 & R_2 & 0 & P_2 \\ 1 & 0 & 0 & \varepsilon_1(\beta_1 - 1) \\ -\beta_2 & 1 & 0 & 0 \end{bmatrix} \begin{bmatrix} x_1 \\ x_2 \\ y_1 \\ y_2 \end{bmatrix} = \begin{bmatrix} x_0F_0 \\ y_3D_3 \\ x_0\beta_1 \\ y_3\varepsilon_2(1 - \beta_2) \end{bmatrix} \quad 13$$

where $\varepsilon_n = \frac{\delta_n}{S+\delta_n-1}$, $\beta_n = (V_n(\delta_n - 1) + 1)^{\frac{1-\delta_n-S}{\delta_n-1}}$, $\delta_n = \frac{D_{n+1}}{P_n}$, $V_n = \frac{P_n}{F_{n-1}}$,

This equation can be solved to obtain values for the unknown concentrations. In turn, these concentrations quantify the solute recovery in the permeate, Y_P, and retentate, Y_R, product streams.

$$Y_P^S = \frac{y_1 P_1}{x_0 F_0} \quad (14)$$

$$Y_R^S = \frac{x_2 R_2}{x_0 F_0} \quad (15)$$

The superscript ^{S} indicates that Equations 8, 14, and 15 are for the stripping section. Equations 9-13 are also unique to the stripping section, but the superscripts are omitted for the sake of clarity.

2.3 Multistage System: Rectifying Section.

Figure 1C shows a rectifying section. In this configuration, the permeate from one stage becomes the feed to the subsequent stage while the retentate is utilized as the diafiltrate. While it retains the same physical interpretation, the definition for the solvent recovery is modified.

$$Y_{w,n}^R = \frac{P_n}{D_{n-1} + F_{n+1}} \quad (16)$$

Subsequently, assuming that the inlet flow rates F_3 and D_0 are known, the flow rates within the rectifying section are derived from mass balances surrounding each stage.

$$R_1 = D_1 = \frac{(1 - Y_{w,1})(D_0 + Y_{w,2} F_3)}{(1 - Y_{w,2} + Y_{w,1} Y_{w,2})} \quad (17)$$

$$P_1 = Y_{w,1} \left(\frac{D_0 + Y_{w,2} F_3}{1 - Y_{w,2} + Y_{w,1} Y_{w,2}} \right) \quad (18)$$

$$R_2 = \frac{(1 - Y_{w,2})(F_3 + (1 - Y_{w,1}) D_0)}{1 - Y_{w,2} + Y_{w,1} Y_{w,2}} \quad (19)$$

$$P_2 = F_2 = Y_{w,2} \left(\frac{(1 - Y_{w,1}) D_0 + F_3}{1 - Y_{w,2} + Y_{w,1} Y_{w,2}} \right) \quad (20)$$

In this configuration, x_0 and y_3 are known concentrations. Species mass balances and Equation 6 results in the linear system of equations below (Supporting Information).

$$\begin{bmatrix} R_1 & 0 & P_1 & -F_2 \\ -D_1 & R_2 & 0 & P_2 \\ 1 & 0 & 0 & -\beta_1 \\ \varepsilon_2(\beta_2 - 1) & 1 & 0 & 0 \end{bmatrix} \begin{bmatrix} x_1 \\ x_2 \\ y_1 \\ y_2 \end{bmatrix} = \begin{bmatrix} x_0 D_0 \\ y_3 F_3 \\ x_0 \varepsilon_1 (1 - \beta_1) \\ y_3 \beta_2 \end{bmatrix} \quad 21$$

where $\varepsilon_n = \frac{\delta_n}{S+\delta_n-1}$, $\beta_n = (V_n(\delta_n - 1) + 1)^{\frac{1-\delta_n-S}{\delta_n-1}}$, $\delta_n = \frac{D_{n-1}}{P_n}$, $V_n = \frac{P_n}{F_{n+1}}$,

The solute recovery in the permeate and retentate product streams can be determined by solving this system of equations.

$$Y_P^R = \frac{y_1 P_1}{y_3 F_3} \quad 22$$

$$Y_R^R = \frac{x_2 R_2}{y_3 F_3} \quad 23$$

The superscript ^{R} indicates that Equations 16, 22, and 23 are for the rectifying section. Equations 17-21 are also unique to the rectifying section, but the superscripts are omitted for the sake of clarity. While only two-stage systems are considered in this study, the approach discussed above can be extended to consider multistage systems with an arbitrary number of stages.

3. Materials and Methods.

3.1 Materials and Chemicals.

An Amicon 8010 (Amicon, Burlington, Massachusetts) stirred cell was used in all diafiltration experiments. NF90 membranes (DuPont, Wilmington, Delaware) were supplied by DuPont. Mass data was recorded on a OHAUS Adventure Series Balance (OHAUS, Parsippany, New Jersey). Pressure data was obtained with an Omega PX409 USBH pressure transducer (Omega, Norwalk, Connecticut). An LFS 1107 Conductivity probe (Innovative Sensor Technology, Las Vegas, Nevada) was used to obtain conductivity measurements. The leads were connected to a current and voltage source using 28 gauge space saver wire (McMaster Carr, Elmhurst, Illinois). PT328 epoxy (Permabond LLC, Pottstow, Pennsylvania) was used as a potting

agent to protect the leads from the saltwater solutions. To make conductivity measurements, a 1 mA peak to peak sinusoidal current was supplied with a Keithly 6221 DC and AC current source function generator (Keithly, Cleveland, Ohio). The voltage drop across the cell was measured using a GwInStek GDS 1054B oscilloscope (GwinStek, Montclair, California). Alternately, the conductivity measurements were made with a CN0359 conductivity measurement system (Analog Devices Incorporated, Thief River Falls, Minnesota) which varies the applied current to maintain a voltage drop equal to 0.7 volts across the electrode. Solutions were prepared with DI water supplied by a Millipore purification system (Milli Q Advantage A10, MilliQ, Massachusetts). Nitric acid and potassium chloride were supplied by Sigma Aldrich (Aldrich, St. Louis, Missouri) and had purities greater than 70% and 99.0%, respectively.

3.2 Hydraulic Permeability Measurements.

The hydraulic permeability of the flat sheet NF90 membrane was determined using a dead end stirred cell. The feed reservoir above the membrane was loaded with 10mL of DI water and pressurized with nitrogen gas. The permeate was collected in a scintillation vial that rested on top of a balance. The time dependent mass and pressure data were logged by a computer. The hydraulic permeability was calculated by taking the average value of three experiments run at pressures ranging from 30 psi and 60 psi.

3.3 Design of Diafiltration Apparatus

The design and operation of the diafiltration apparatus has been described within our previous work.[33] In summary, the apparatus seen within Figure S1 modifies a dead-end filtration stirred cell to introduce a diafiltrate solution into the retentate at a volumetric flux equal to that of the permeate crossing the membrane. The scintillation vial sits on an OHAUS balance that is

connected to a computer which records the time dependent mass. The in-situ retentate concentration is monitored through an inline conductivity probe. While measurements with the Keithly 6221 DC and AC current source function generator and GwInStek GDS 1054B oscilloscope are manually made by the experimenter, the Analog CN0359 conductivity board allows for automated recording of the retentate data at predetermined time intervals.

3.3 Diafiltration Experiments

Experiments were conducted within the aforementioned diafiltration apparatus. 5 mL of DI water were passed through the membrane at an applied pressure of 60 psi before all experiments. 200 mL of diafiltrate solution were prepared and loaded into the diafiltrate tank. 1 mL of the diafiltrate solution was stored in a scintillation vial for further analysis by ICP-OES (inductively coupled plasma optical emission spectroscopy). 11 mL of feed solution was added to the stirred cell volume above the membrane. The stirred cell was placed on a magnetic stir plate for 10 minutes to allow ions to adsorb onto the membrane and exposed stirred cell surfaces. 1 mL of the feed solution was removed from the stirred cell and stored within a scintillation vial for analysis by ICP-OES. Recording the weight of the feed solution allowed for mass balance calculations to corroborate the measured retentate conductivity measurements.

At the start of the experiment, the volume of air in the tubing between the diafiltrate supply tank and the stirred cell must be compressed into the headspace of the stirred cell. This process, which brings the diafiltrate solution to the entrance of the stirred cell, is achieved experimentally by pressurizing the stirred cell and diafiltrate tank to 1/6 of the operating pressure. Once this initial pressure was reached, the three-way valve was switched to pressurize the diafiltrate tank to an operating pressure of 60 psi. A conductivity reading was taken immediately after the system reached the operating pressure. Additional readings were taken at approximately 30-minute

intervals. A rubber tube fed the permeate into scintillation vials that rested on top of a balance. Scintillation vials were collected in 1 mL intervals and stored for further analysis by ICP-OES. During the experiment, a computer was used to track the time dependent mass and pressure data.

The system was shut down by closing the main nitrogen supply valve and then opening the pressure relief valve on the diafiltrate tank. Depressurizing the system in this way allows the air in the headspace of the stirred cell to expand and push the diafiltrate solution through the tubing and back into the diafiltrate tank. The permeate solution within the tube between the stirred cell and scintillation vial as well as the retentate solution were collected in separate scintillation vials and stored for future analysis.

3.3 ICP-OES Sample Preparation and Analysis

ICP-OES measurements were conducted on a Perkin Elmer Avio 200. 100 µL of each sample was added to 15 mL centrifuge tubes and diluted with 5 mL of 3% nitric acid. The concentration of potassium chloride within the samples were interpolated using calibration curves with a minimum correlation coefficient of 0.99.

3.3 Conductivity Sensor Calibration

The LFS 1107 conductivity probe was calibrated for both manual use with the Keithly 6221 DC and AC current source function generator and GwInStek GDS 1054B oscilloscope as well as for semi-continuous data recording with the CN0359 Analog conductivity board. Both calibration curves (Figure S2) were made with a minimum of 7 calibration standards and presented correlation coefficients greater than 0.99. All experimental data were interpolated using the appropriate curve.

4. Results and Discussions

4.1 Identification and Experimental Validation of a Critical Diafiltrate Flux

Prior to comparing the experimental results and model predictions for a diafiltration stage, it is useful to contemplate how the retentate concentration can evolve as solution permeates through the membrane. In particular, by taking the derivative of the concentration profile (Equation 6) with respect to V and setting it equal to zero an expression that describes a critical value δ^* is identified.

$$\delta^* = \frac{S-1}{G-1} \tag{24}$$

At δ^*, the flux of solute into the retentate balances the flux of solute out, and its concentration remains constant as the volume of solution recovered increases. If this constraint is not met, the solute concentration will change along the length of the module. For $\delta < \delta^*$, the solute flux into the retentate is greater than its flux out. Thus, the solute concentration in the retentate increases with V. In the other limit, $\delta > \delta^*$, the retentate concentration decreases with V as the diafiltrate dilutes the retentate.

The results of experiments to explore the diluting, critical, and concentrating regimes of operation are presented in Figure 2. A 10 mM KCl feed solution was used in all of the experiments as it was high enough to observe dilution in the diluting regime, yet low enough to avoid high osmotic pressures in the concentrating regime. Preliminary KCl rejection experiments suggested S ~ 0.18 for the single membrane type (NF-90) utilized in these experiments. As such, in order to explore the operating regimes, the value of δ^* was modulated by adjusting the ratio of the diafiltrate to feed concentration. To operate at the critical condition, $\delta = \delta^* = 1 = \frac{S-1}{G-1}$, G must equal the sieving coefficient, S. Experimentally, $\delta = \delta^*$ conditions were explored using two

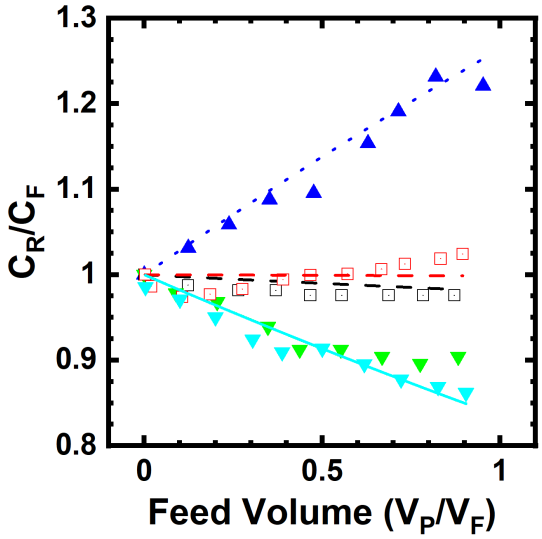

Figure 2. A comparison of experimental data and model predictions for a single-stage diafiltration module. Experimental concentration data for the retentate solution in the concentrating (upward-facing blue triangles), critical (black and red hollow squares) and diluting (downward-facing green and cyan triangles) regimes were measured using an inline conductivity probe (The complete data sets from the inline conductivity probe are presented in Figure S4). Theoretical predictions for the concentrating, critical, and diluting regimes (dotted, dashed, and solid lines, respectively) were generated using Equation 7 and a sieving coefficient of 0.185. Diafiltrate concentrations of 5 mM and 0 mM KCl were used for the concentrating and diluting regimes, respectively. In the critical regime, the experiment with a diafiltrate concentration of 1.5 mM KCl is presented as hollow black squares and the experiment with a 1.8 mM KCl diafiltrate concentration is presented as hollow red squares. In all experiments, the retentate concentration is normalized with respect to the initial feed concentration of 10 mM KCl. The mass of permeate collected is normalized by the initial volume of the feed solution, 10 mL. The volume of permeate is obtained from mass data and a constant density is assumed. All experiments were run until the total volume of permeate collected was approximately equal to one feed volume.

diafiltrate solutions with concentrations of 1.5 mM KCl (hollow black squares) and 1.8 mM KCl (hollow red squares). The diluting regime was achieved by using a DI water diafiltrate (G = 0) such that δ^* = 0.815. The results from these experiments are shown as downward-facing triangles in Figure 2. The retentate concentration decreases since there is no KCl in the diafiltrate to replenish the solute permeating across the membrane. A 5 mM KCl diafiltrate solution was used to operate in the concentrating regime. Here, $G = 0.5$ leading to δ^*= 1.63. In this regime, solute from the high concentration diafiltrate is added at a rate greater than the rate solute permeates

across the membrane. This feature is evident as the retentate concentration indicated by the upward-facing blue triangles in Figure 2 increases throughout the course of the experiment.

The aforementioned diafiltration apparatus works on the premise that $J_w = J_D$, i.e., δ = 1. Thus, Equation 7 was used to predict the retentate concentration. Nonlinear regression of the five experimental data sets shown in Figure 2 identified one unique sieving coefficient, $S = 0.181 \pm 0.005$, could fit the data accurately. Specifically, the dotted, dashed, and solid lines shown in Figure 2 correspond to predictions for the concentrating, critical, and diluting operating regimes, respectively. Figure S3 demonstrates the 95% confidence interval for these predictions (based on the uncertainty in the regressed parameter *S*). On average, experimental data and theoretical prediction are within 1.6%. The maximum difference between the model predictions and experiments remains within 10%. The largest deviations occur for the diluting regime experiment where conductivity measurements were obtained using the oscilloscope (downward facing green triangles). Continuous conductivity data from the Analog Device (downward facing cyan triangles) reduced the deviation to 3.5%. As such, the deviation is believed to arise, in part, from the accuracy of the conductivity measurement devices. This idea is supported by the data within Figure S2, which demonstrates that the linear region of the calibration curve for the oscilloscope does not extend to concentrations below 5mM. Figure S5 corroborates this information as it demonstrates how analogous retentate concentration measurements can be calculated using experimental measurements of the permeate concentration in conjunction with mass balances. Moreover, the model predicts the KCl concentration in the permeate samples reasonably well as demonstrated by Figure S6.

4.2 Configuration of Multistage Cascades Determines Solute Recovery Profile

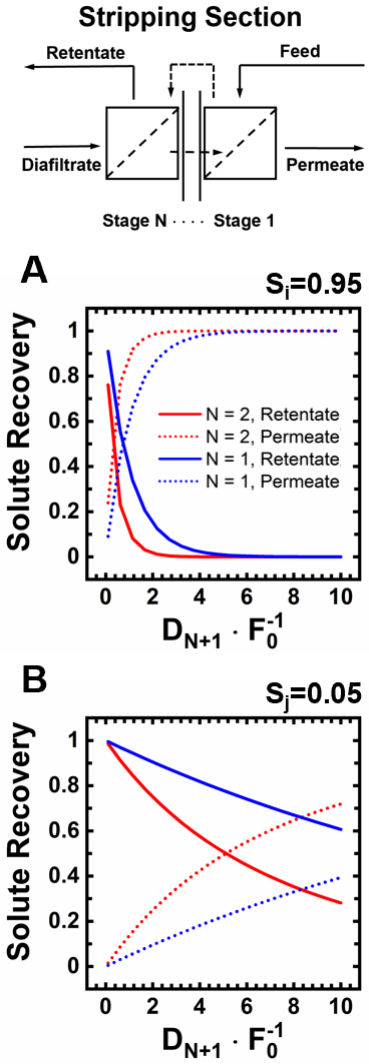

Figure 3. Solute recovery as a function of D/F for a stripping section. (**A**) and (**B**) present the variations in recovery for solutes that have sieving coefficients of 0.95 and 0.05, respectively. Solute recovery in the permeate is represented by the dotted lines. Permeate recovery for a single-stage stripping configuration can be calculated using Equation SI6. Permeate recovery data for the two-stage stripping configuration is calculated using Equation 14. For a two-stage stripping configuration, the retentate recovery is calculated using Equation 15. Solute recovery in the retentate is indicated by the solid lines. All the calculations assume an initially pure diafiltrate.

Based on its predictive capabilities, the model for a single diafiltration stage was extended to analyze multistage designs. In this section, the designs considered assume constant molar

overflow such that $^{D}/_{F}$ is constant for all the stages in a cascade. This constraint impacts the two operating configurations differently. Within the stripping section, $D = P$. Thus, for $^{D}/_{F}$ to be constant, $\delta = 1$, $V = {}^{D_3}/_{F_0}$, and $Y_{w,1}^{S} = Y_{w,2}^{S} = \frac{P}{F+D} = \frac{{}^{D_3}/_{F_0}}{1+{}^{D_3}/_{F_0}}$. For the rectifying section, $F = P$. Consequently, at constant $^{D}/_{F}$, $\delta = {}^{D_0}/_{F_3}$, $V = 1$, and $Y_{w,1}^{R} = Y_{w,2}^{R} = \frac{P}{F+D} = \frac{1}{1+{}^{D_0}/_{F_3}}$.

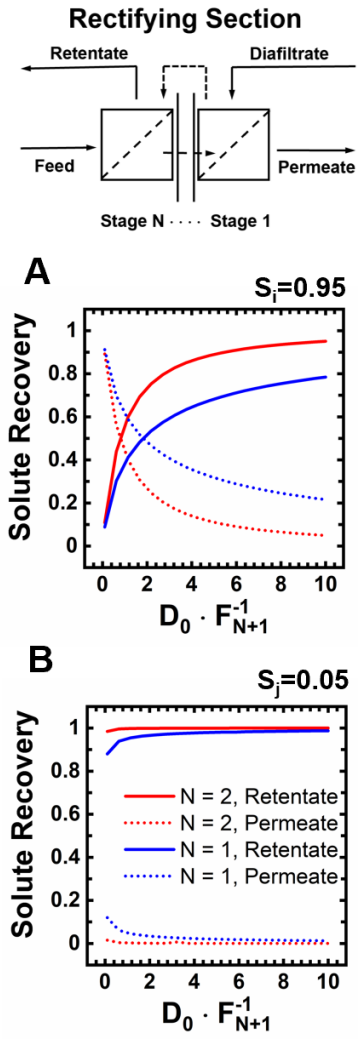

Figure 4. For the rectifying section configuration, (**A**) and (**B**) report the effect of $^{D}/_{F}$ on the recovery of solutes that have sieving coefficients of 0.95 and 0.05, respectively. Solute recovery in the permeate is represented by the dotted lines. The two-stage permeate recovery is calculated using Equation 22. The single-stage retentate recovery is calculated using Equation SI7. The two-stage retentate recovery is calculated using Equation 23. Solute recovery in the retentate is indicated by the solid lines. All the calculations assume an initially pure diafiltrate.

Figure 3 and 4 examines the recovery of two solutes within diafiltration processes subject to these constraints. In this analysis, the more permeable solute has a sieving coefficient of $S_i = 0.95$. The less permeable solute has a sieving coefficient $S_j = 0.05$. Percent rejection can be calculated as $1 - S$ such that solute *i* is 5% rejected and solute *j* is 95% rejected. It should be noted that all of the trends described below result from the connectivity of the systems since the membrane properties are held constant in the analysis. In all the panels, solute recovery in the retentate is indicated using solid lines and solute recovery in the permeate is denoted using dotted lines. The blue lines correspond to a single-stage diafiltration unit while the red lines correspond to a two-stage diafiltration cascade. Figure 3A and 3B examine recovery for a stripping section and Figure 4A and 4B for a rectifying section.

Because increasing D/F corresponds to an increase in solvent recovery for a stripping section, this design configuration is more efficient at recovering solute within the permeate stream. For example, in Figure 3A the rapid increase in the recovery of solute *i* in the permeate product can be attributed to the larger volume of solution permeated. For the solute to be recovered within the permeate, it must be removed from the retentate. Thus, the retentate recovery decreases as D/F increases. Similar trends are observed in Figure 3B for the recovery of solute *j* ($S_j = 0.05$). The decrease in the initial slopes of these lines is a consequence of solute *j* being less permeable.

Notably, at a given D/F value, increasing the number of stages within the stripping configuration allows for a higher recovery of solute in the permeate. This trend can be explained by referring to the illustration at the top of Figure 3. Any solute that is rejected in the first stage passes into the second stage as the feed solution. Consequently, the solute that permeates through

the membrane in stage 2 is reintroduced back into the first stage as the diafiltrate, providing an additional opportunity for the solute to be recovered within the final permeate product.

The trends in solute recovery with increasing $^{D}/_{F}$ are inverted for the rectifying section configuration relative to the stripping section. That is, as shown in Figure 4A and 4B, the recovery of solute within the permeate stream decreases with increasing $^{D}/_{F}$ while the recovery of solute within the retentate increases. These results can be rationalized with the help of two mathematical relationships. First, in the rectifying section, an increase in $^{D}/_{F}$ corresponds to a decrease in the solution recovery, $Y_{w,1}^{R} = Y_{w,2}^{R} = \frac{1}{1+{}^{D_0}/_{F_3}}$. Additionally, introducing larger volumes of diafiltrate dilutes the local solute concentration, which in accordance with how J_s is expressed in Equation 4, reduces the flux of solute across the membrane. The smaller volume of solution recovered and lower driving force for solute transport combine to reduce solute recovery in the permeate stream.

For the rectifying section design, at a fixed $^{D}/_{F}$ value, increasing the number of stages leads to a higher recovery of solute within the retentate. Similar to the explanation provided for the stripping section, this trend is rationalized by the increased number of opportunities that a given solute has to be retained within the retentate stream. As displayed within the Figure 4 illustration, solutes that permeate through the second stage have the potential to be rejected by stage 1 and reintroduced into stage 2 as the diafiltrate.

The differences in the performances of the two designs can be directly contrasted by controlling for the solvent recovery. Specifically, when operating at $^{D}/_{F} = 1$, both configurations have a $Y_{w,n}^{R} = Y_{w,n}^{S} = 0.5$. At these conditions, the multistage stripping configurations show larger recoveries within the permeate when compared to the multistage rectifying configuration. For

example, a single-stage provides an equivalent permeate recovery of 61.3% for solute *i* in both configurations. As the number of stages increases, the connectivity of the stages directs the solute into different effluent streams. The two-staged stripping section provides permeate recoveries of solute *i* equal to 89.2% whereas the two-staged rectifying section provides recoveries of solute *i* in the permeate equal to 43.5%. A similar analysis shows that multistage rectifying modules perform better than multistage stripping modules in capturing solute within the retentate. Further increases in the number of stages enhance these trends identified when transitioning from a single-stage to a two-stage system.[27,28]

4.3 Recovery-Purity Trade-offs Highlight Applications for Multistage Configurations

Solute purity within the product streams was also examined as a function of the operating conditions. Here, purity was calculated as the fraction of the target solute recovered in an effluent stream with respect to the total amount of solute recovered in that stream. For example, as demonstrated in Equation 27, the purity of solute *i* within the permeate stream, $\alpha_{P,i}$, is expressed in terms of the recovery of solute *i* and solute *j* in the permeate, $Y_{P,i}$ and $Y_{P,j}$, respectively.

$$\alpha_{P,i} = \frac{Y_{P,i}}{Y_{P,i} + Y_{P,j}} \tag{27}$$

The results of this analysis are reported in Figure 5.

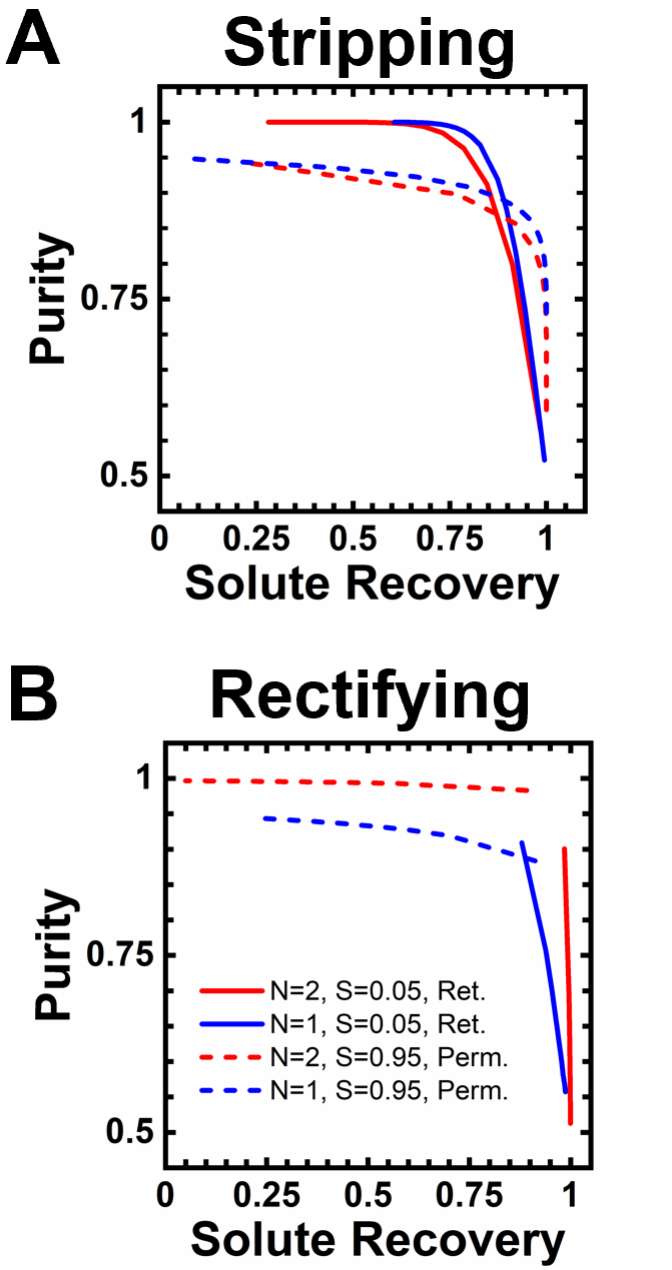

Figure 5. Solute purity plotted versus solute recovery for a stripping section (**A**) and a rectifying section (**B**). The values reported are for the stream where the solute is more likely to be recovered. For example, it is anticipated that the more permeable solute ($S_i = 0.95$) will be recovered within the permeate. The dotted lines correspond to the purity and recovery of solute *i* within the permeate streams. The solid lines correspond to the purity and recovery of solute *j* ($S_j = 0.05$) within the retentate streams. Purity was calculated with equations analogous to Equation 27.

Figure 5A and 5B present the solute purity as a function of its recovery for the stripping and rectifying section configurations, respectively. Figures that display the purity of a species as a

function of $^{D}/_{F}$ are included within the Supporting Information (Figure S7). For each species, the purity values are reported for the stream in which it is expected to be recovered. Specifically, it is assumed that the more permeable species, $S_i = 0.95$, will be recovered preferentially within the permeate effluent and thus the dotted lines correspond to its purity and recovery in the permeate. The solute with a sieving coefficient of $S_j = 0.05$ will be highly rejected by the membrane and primarily recovered in the retentate. Therefore, the solid lines correspond to its purity and recovery in the retentate stream. As before, the blue lines correspond to a single-stage operation while the red lines correspond to a two-stage process. Generally speaking, the retentate stream of the stripping configuration has a higher purity than the permeate stream. Similarly, the permeate stream of the rectifying section exhibits higher purities than the retentate stream. These observations suggest that similar to the permeability-selectivity tradeoff for materials, there is a process-based trade-off where the solute purity in the effluent streams decreases with increasing solute recovery.

Within the stripping configuration, at a constant purity, the recovery of solute decreases as the number of stages increases. This observation is directly related to the rapid increase in the recovery of both solutes in the permeate stream shown in Figure 3A and 3B. As the number of stages increases, so does the probability that the rejected solute ($S_j = 0.05$) is lost to the permeate stream. Consequently, the purity of the solute *i* in the permeate stream decreases as the number of stages increase. In contrast, for the rectifying section configuration at a fixed purity, solute recovery increases as the number of stages increases. The high purity of the permeate is driven by the decreasing likelihood that a solute with a low sieving coefficient will pass through the membrane multiple times.

These insights regarding the recovery and purity of species suggest heuristics that can help guide whether the stripping or rectifying configuration is more appropriate for a specific separation. The high recoveries that can be achieved at low $^{D}/_{F}$ values using a stripping section configuration are attractive for separating solutes with finite sieving coefficients from solutes that exhibit a sieving coefficient equal to zero (e.g., buffer exchange). In this way, the configuration can effectively wash out impurities from a high value solute. In fact, recent literature demonstrates staged diafiltration cascades as an enabling technology for continuous biopharmaceutical processing. [27,28]

A comparison between this work and the prior studies that utilized a stripping section configuration for the formulation of valuable biological therapeutics reveals several design considerations (e.g., module configuration, membrane selection) that may enable further improvements to staged diafiltration processes.[23] First, in the prior studies commercially available diafiltration modules were utilized to generate staged cascades. These modules could be modelled by assuming the feed and diafiltrate streams were mixed prior to being introduced to a membrane module as a blended solution.[28] This approach, which repeatedly diluted and subsequently reconcentrated the solutes, lowers the driving forces for solute transport by reducing its local concentration. As illustrated within Figure 1A, the design considered within this work systematically introduces diafiltrate over the length of the module, which keeps the local solute concentration higher. In turn, higher driving forces for solute transport allow for comparable recoveries to be achieved at lower $^{D}/_{F}$ values thus offering the potential to reduce the volume of diafiltrate consumed. The opportunity to reduce the diafiltrate demand by operating at higher solute concentrations was highlighted in the prior literature, which also indicated the complexities that may arise with such an approach (e.g., protein gelation and membrane fouling). In

combination, these observations suggest that there may be opportunities for innovative module designs that are tailored for use in staged diafiltration processes. In particular, modules that allow for diafiltrate to be dosed continuously along their length enable operations in diluting, critical, and concentrating regimes that may help to mitigate the limiting effects of fouling or gelation while utilizing less diafiltrate solution. Toward this aim, additive manufacturing has already begun to enable the development of innovative modules that increase separation efficiency of membrane chromatography[34–37] and single-stage diafiltration operations.[31,38]

The solute pair analyzed here highlights the importance of selecting membranes capable of fully rejecting target solutes to maintain high recoveries and purities when implementing a stripping section configuration. This need is highlighted by the rapidly increasing recovery of solute *j* within the permeate stream of Figure 3B. Even though it is rejected at a relatively high rate, 95%, its recovery increases quickly due to the connectivity of stages within the cascade. This consideration was addressed in the prior studies where low molecular weight impurities, represented by vitamin B12 ($S \sim 1$), were removed from valuable components (i.e., monoclonal antibodies and other therapeutic proteins) with high molar masses ($S = 0, \%R = 100\%$) using a membrane with a molecular weight cut-off of 30 kDa, which is well below the size of the valuable biological species.

Alternatively, when both solutes have sieving coefficients that fall between 0 and 1, the rectifying configuration enhances the fractionation of the solutes. This approach has utility in the emerging precision separations where solutes of similar molecular size and chemistry must be fractionated (e.g., purifying rare earth elements[39], recovering nutrients from wastewater[4,5], or recycling lithium-ion batteries[8,40]). Notably, when compared to its stripping section counterpart, a single-stage rectifying section can offer increased purities at high recoveries. More importantly,

the rectifying configuration exploits the advantages of staging to simultaneously improve solute recovery and purity with the addition of each subsequent stage.

4.4 Asymmetric Operations Provide Opportunities to Improve Solute Recovery and Purity

Asymmetric cascades, where each stage operates at a different $^{D}/_{F}$ ratio, have the potential to improve the recovery and purity of solutes relative to cascades operating at constant $^{D}/_{F}$. The following discussion examines these trends by focusing on solutes with sieving coefficient of $S_i = 0.8$ and $S_j = 0.2$. For reference, graphs analogous to Figures 3-5 and S7 that examine the recovery and purity of these two solutes for constant $^{D}/_{F}$ systems are presented in the Supporting Information (Figures S8 – S11). Figure 6A presents a contour map for the purity of solute j ($S_j = 0.2$) in the retentate as a function of the solvent recovery for a two-stage stripping configuration. $Y_{w,1}$ and $Y_{w,2}$ are the solvent recovery for stage 1 and in stage 2, respectively. The permeate purity of solute i ($S_i = 0.8$) as a function of solvent recovery is presented in Figure 6B. The contours were generated at a constant influent ratio $^{D_3}/_{F_0} = 1$. Asymmetric operating conditions are then realized by varying the recovery of solvent for each stage. A symmetric system in which both stages operate with $^{D}/_{F} = 1$ occurs when $Y_{w,1} = Y_{w,2} = 0.50$. This unique condition is represented by the red circle in Figure 6.

For the stripping section configurations, the distinct orientation of the contour lines for the permeate purity (Figure 6B) relative to the contour lines for the retentate purity (Figure 6A) and recovery (Figures S12-S14), can allow for increased solute purity and recovery using asymmetric systems. Notably, in the region of interest near the red circle, the contour lines in Figure 6B are aligned vertically while the contours in the remaining plots are aligned diagonally from top left to

bottom right. As such, movement along a retentate iso-purity contour can increase the purity of

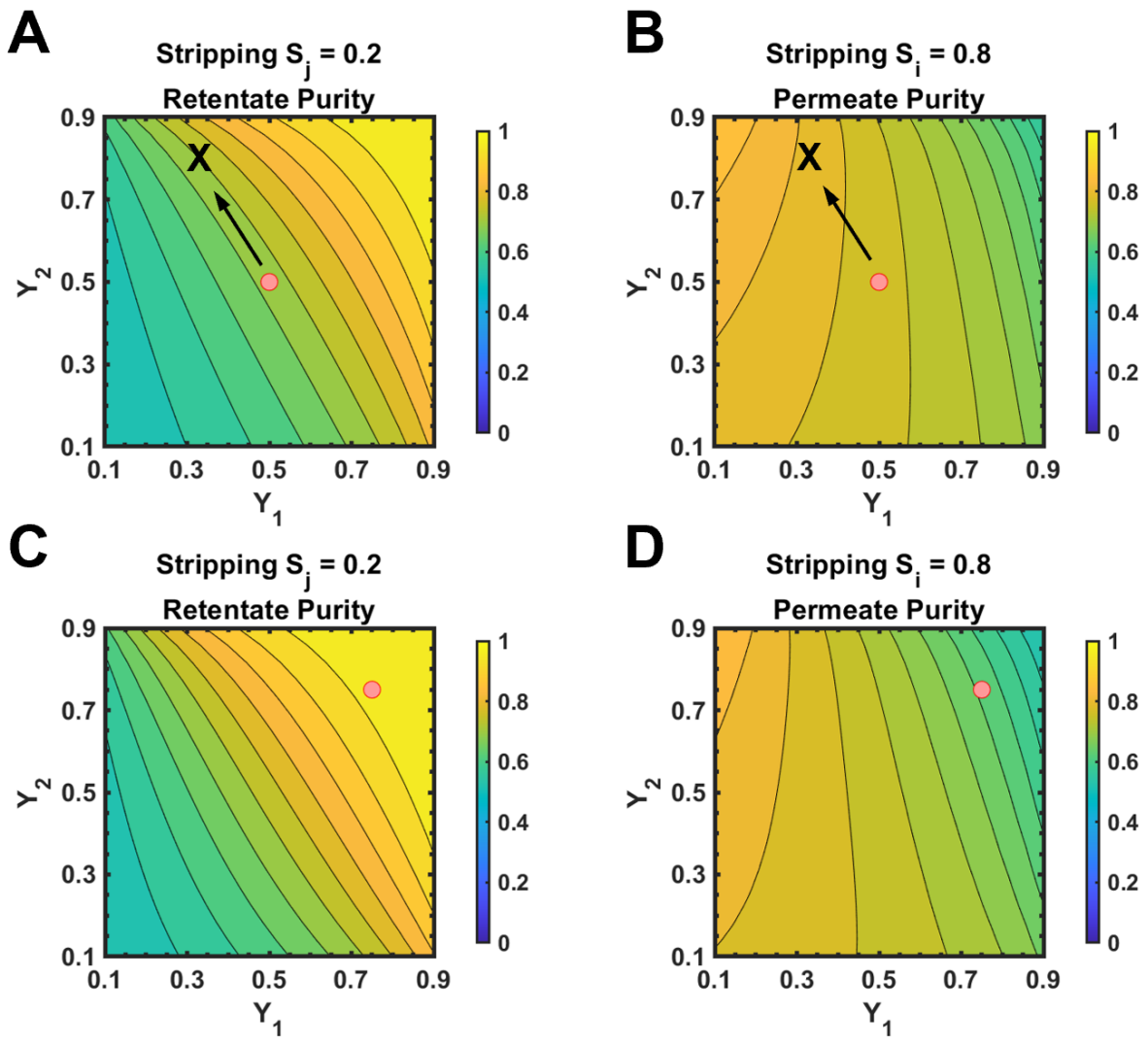

Figure 6. (**A**) A contour map for the purity of solute *j* ($S_j = 0.2$) in the retentate product of a two-stage stripping section. Purity is plotted as a function of the solvent recovery in stage 1, *Yw,1*, and stage 2, *Yw,2*. (**B**) The purity of solute *i* ($S_i = 0.8$) in the permeate product as a function of solvent recovery for the same two-stage stripping section. All the cascade designs considered had an inlet flow ratio ${}^{D_3}/_{F_0} = 1$. The red circle corresponds to a system operating at a constant ${}^{D}/_{F} = 1$, $Y_{w,1} = Y_{w,2} = 0.50$. Moving from the red circle to the **'X'** highlights an asymmetric operation that can increase the purity of a specific stream. (**C**) and (**D**) Contour maps for the purity of solute *j* in the retentate product and solute *i* in the permeate product, respectively. All designs had an inlet flow ratio ${}^{D_3}/_{F_0} = 3$. The red circle corresponds to a symmetric system operating at a constant ${}^{D}/_{F} = 3$, $Y_{w,1} = Y_{w,2} = 0.75$.

the permeate. For example, within a symmetric system that operates at a constant $^{D}/_{F} = 1, Y_{w,1} = Y_{w,2} = 0.50$, the purity of solute *j* in the retentate (Figure 6A) is ~70% and the purity of solute *i* in the permeate (Figure 6B) is ~77%. Asymmetric operations can be achieved by following the 70% retentate iso-purity contour line (represented by the black arrow) towards the '**X**'. Physically, the asymmetric system decreases the recovery of solvent in stage 1 and increases the recovery of solvent in stage 2. Within Figure 6B, this maneuver crosses the contour lines of the permeate purity, increasing the purity of solute *i* to 84%. The increase in the permeate stream purity occurs because an increase in the solvent recovered through stage 2 corresponds to an increase in the recovery of solute *i* in the permeate (Figure S13E). On the contrary, the contours presented in Figure S13D show that the increased solvent recovery of stage 2 has little effect on the recovery of solute *j* in the permeate.

Figure 6C and 6D present similar data yet the red circle considers a system operating at $^{D_3}/_{F_0} = 3$ such that constant $^{D}/_{F}$ conditions occur at $Y_{w,1}^{S} = Y_{w,2}^{S} = 0.75$. Here, no asymmetric cascade provides clear performance gains relative to the constant $^{D}/_{F}$ conditions as noticeable trade-offs between increasing the purity or recovery of solute must be balanced. For example, moving horizontally to the left (i.e., decreasing solvent recovery in stage 1) leads to a decrease in the purity of the retentate (Figure 6C) and an increase in the purity of the permeate (Figure 6D). Likewise, there is little gain by moving vertically.

Similar graphs exploring the improved purities and recoveries of asymmetric rectifying configurations provide insights into designing this class of cascade. Figure 7A and 7C report the recovery of solute *i* in the retentate and permeate product streams, respectively. To better elucidate

the opportunities for asymmetric rectifying sections, the values reported are the solute recovery at

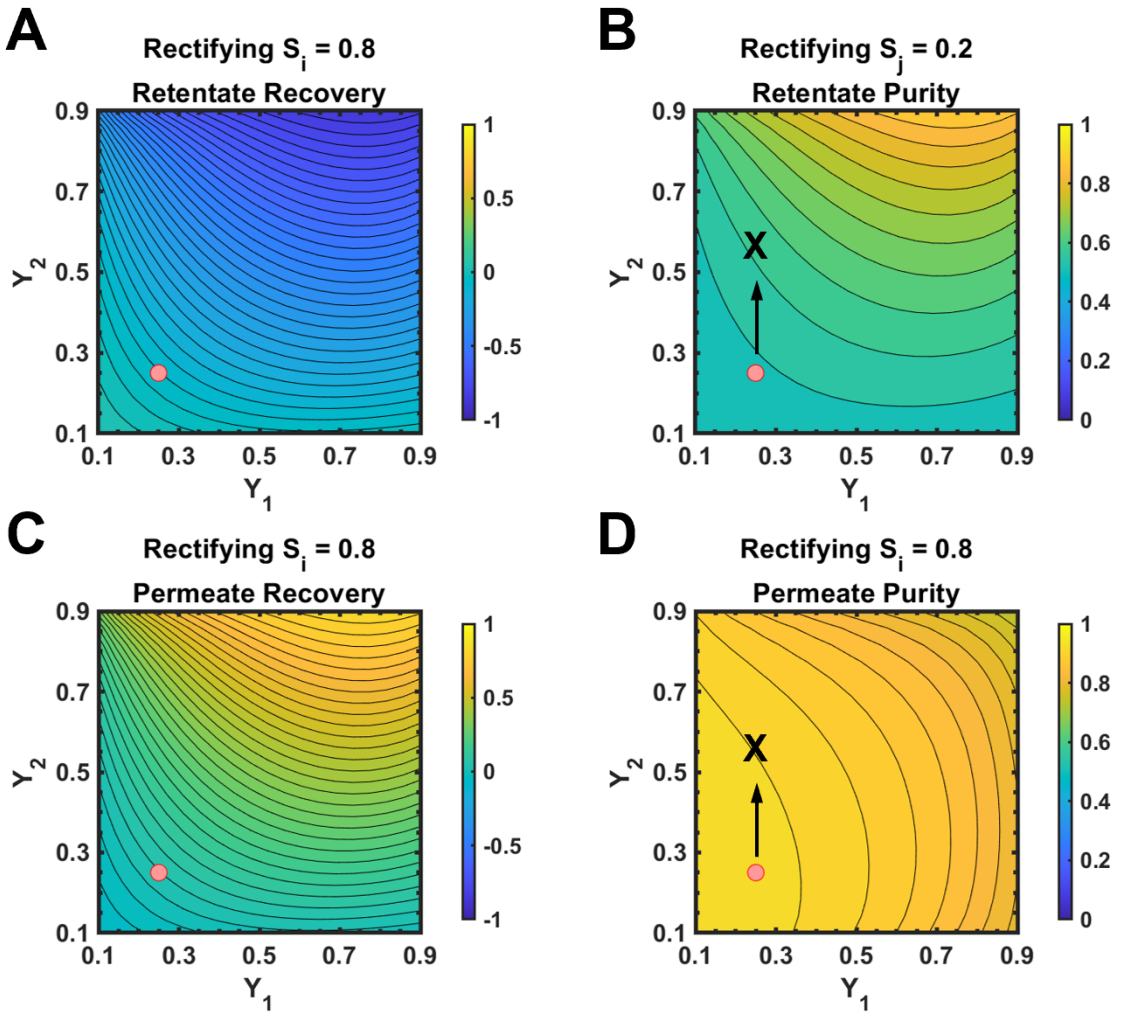

Figure 7. (**A**) A contour map for the recovery of solute *i* ($S_i = 0.8$) in the retentate product of a two-staged rectifying section. Recovery is plotted as a function of the solvent recovery in stage 1, $Yw_{,1}$, and stage 2, $Yw_{,2}$. (**C**) A contour map for the recovery of solute *i* ($S_i = 0.8$) in the permeate product. All the designs considered had an inlet flow ratio of $^{D_0}/_{F_3} = 3$. The solute recoveries in (**A**) and (**C**) are reported relative to the solute recovered for a system operating at a constant $^{D}/_{F} = 3$, $Y_{w,1} = Y_{w,2} = 0.25$. The red circle indicates the position where this variable is equal to zero. (**B**) The purity of solute *j* ($S_j = 0.2$) in the retentate product stream. (**D**) The purity of solute *i* ($S_i = 0.8$) in the permeate product stream. Operating at a constant $^{D}/_{F} = 3$, the purity of solute *j* in the retentate is equal to 53%. Likewise, the purity of solute *i* in the permeate stream is equal to 92%. The purities within (**B**) and (**D**) were calculated using equations analogous 27. Following the arrow from the red circle towards the **'X'** demonstrates how a move from symmetric operations to an asymmetric system can results in an increase in the purity of the retentate at little cost to the purity of the permeate.

a given operating condition minus the solute recovery for a constant $^{D}/_{F} = 3$ operation. Figure 7B and 7D presents the purity of solute *j* in the retentate product and solute *i* in the permeate effluent, respectively. The red circle represents a system operating at $Y_{w,1}^{S} = Y_{w,2}^{S} = 0.25$ such that constant $^{D}/_{F} = {}^{D_0}/_{F_3} = 3$ conditions occur. Within Figure 7B, the vertical black arrow demonstrates how increasing the solvent recovery of the second stage can increase the retentate purity from 53% to 56%. This increase in the purity of the retentate comes at a low cost in the permeate purity (i.e., a decrease from 92.7% to 92.0%). Physically, the increased purity is realized by increasing the recovery of solute *i* in the permeate (Figure 7C). Similar figures that report the unadjusted recovery of solute as a function of the solvent recovery in both stages are presented within Figure S15. Figures S15A, S15D show that operating under these asymmetric conditions has little effect on the recovery of solute *j*.

Figure 8 is analogous to Figure 7, yet it examines a staged rectifying module run at a constant $^{D_0}/_{F_3} = 0.33$. As such, a constant $^{D}/_{F} = 0.33$ operation occurs at $Y_{w,1}^{S} = Y_{w,2}^{S} = 0.75$ (red circle). Beginning at symmetric operating conditions, it can be advantageous to move along the permeate iso-purity contour line of 87%. By following the black arrow towards the '**X**' the purity of the retentate stream is increased up to 91%. Since utilizing these asymmetric operating conditions leads to no appreciable change in the recovery of solute *j* in the permeate or retentate (Figure S17A and S17D), the increased purity of the retentate is due to the increase in the recovery of solute *i* in the permeate (Figure 8C).

The same analysis as discussed above can be conducted for solutes with sieving coefficients of 0.05 and 0.95. These figures are provided in the Supplementary Information (Figures S18-S23).

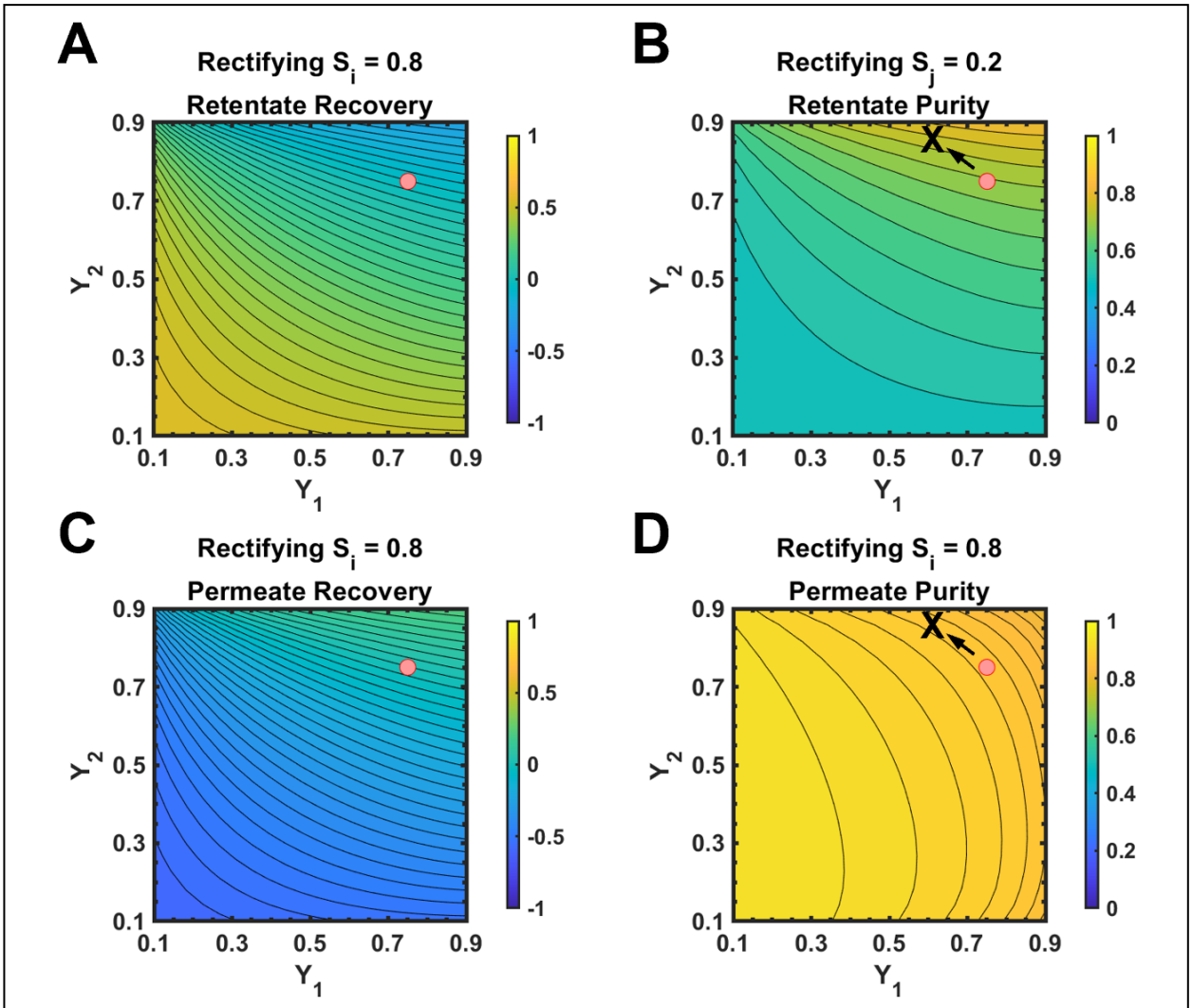

Figure 8. (**A**) A contour map for the recovery of solute *i* ($S_i = 0.8$) in the retentate product of a two-staged rectifying section. Recovery is plotted as a function of the solvent recovery in stage 1, $Yw_{,1}$, and stage 2, $Yw_{,2}$. (**C**) A contour map for the recovery of solute *i* ($S_i = 0.8$) in the permeate product. All the designs considered had an inlet flow ratio of $^{D_0}/_{F_3} = 0.33$. The solute recoveries in (**A**) and (**C**) are reported relative to the solute recovered for a system operating at a constant $^{D}/_{F} = 0.33$, $Y_{w,1} = Y_{w,2} = 0.75$. The red circle indicates the position where this variable is equal to zero. (**B**) The purity of solute *j* ($S_j = 0.2$) in the retentate product stream. (**D**) The purity of solute *i* ($S_i = 0.8$) in the permeate product stream. Operating at a constant $^{D}/_{F} = 3$, the purity of solute *j* in the retentate is equal to 73%. Likewise, the purity of solute *i* in the permeate stream is equal to 87%. The purities within (**B**) and (**D**) were calculated using equations analogous to 27. Following the arrow towards the **'X'** corresponds to moving to asymmetric operations that can increase the purity of a specific stream, in this case, that of the retentate.

The asymmetric conditions identified here increased solute purity for both operating configurations by increasing the solvent recovery of stage 2 and decreasing the solvent recovery of stage 1. The permeate from stage 1, P_1, is an effluent stream that is not reintroduced into the cascade. Reducing $Y_{w,1}$, reduces P_1, which results in more solute being redirected back into the cascade. Conversely, increasing solvent recovery for stage 2 reduces the relative volume of the effluent stream R_2 by increasing P_2, which provides the solution with additional opportunities to recirculate through the cascade. Therefore, in a manner analogous to how increasing the number of stages promoted increased recoveries, asymmetric operations engender increased permeate purity in the stripping section and increased retentate purity in the rectifying section. These asymmetric operating conditions exemplify how the design of systems can increase effluent purity and solute recovery without solely depending on material advancements.

5. Conclusion

Innovations at the materials, device, and systems scales need to occur in tandem to propel membrane separations forward. In this study, this need was highlighted by developing a mathematical model for staged diafiltration processes. After experimentally validating the model at the single-stage scale, it was extended to consider the design of multistage stripping and rectifying section configurations. The stripping section configuration performs well when low molar mass impurities need to be removed from large, impermeable solutes, a situation similar to buffer exchange in the processing of biological therapeutics. Alternatively, the rectifying section configuration has a unique ability to separate multiple solutes that possess sieving coefficients between zero and one, this ability could be useful in emerging applications such as the isolation of rare earth elements, the recovery of resources, and the recycling of lithium-ion batteries. Notably, by holding the membrane properties constant, this analysis reinforces that these opportunities arise

due to the connectivity of the system, not strictly material properties. For the module design considered here, a critical diafiltrate flux that maintains the retentate concentration at a constant value throughout the course of an experiment was identified. This finding suggests module design can be used to enhance diafiltration performance. In particular, processes that are able to maintain larger driving forces for solute transport utilize less diafiltrate to accomplish the desired separation. Maintaining high concentrations and large driving forces with existing staged diafiltration modules, which repeatedly dilute and reconcentrate the solutes, is complicated by phenomena such as gelation, scaling, and fouling. Thus, enabled by additive manufacturing, there may be significant opportunities to develop diafiltration modules that provide more control over the evolution of the solute concentration profiles.

Nomenclature

Symbol	Meaning	Unit
A_c	Cross-sectional area	m^2
a_m	Packing density	m^{-1}
c_1	Molar concentration	$\mathrm{mol} \cdot \mathrm{L}^{-1}$
D	Diafiltrate flow rate	$\mathrm{m}^3 \cdot \mathrm{s}^{-1}$
F	Feed flow rate	$\mathrm{m}^3 \cdot \mathrm{s}^{-1}$
G	Concentration ratio of diafiltrate to feed	Dimensionless
J	Volumetric flux	$\mathrm{m}^3 \cdot \mathrm{s}^{-1} \cdot \mathrm{m}^{-2}$
N	Normalized percent recovery	Dimensionless
P	Permeate flow rate	$\mathrm{m}^3 \cdot \mathrm{s}^{-1}$
R	Retentate flow rate	$\mathrm{m}^3 \cdot \mathrm{s}^{-1}$
S	Sieving coefficient	Dimensionless

V	Feed volume	Dimensionless
v^0	Fluid velocity	$\mathrm{m \cdot s^{-1}}$
x	Molar concentration of membrane overflows	$\mathrm{mol \cdot L^{-1}}$
Y	Percent recovery	Dimensionless
y	Molar concentration of membrane underflows	$\mathrm{mol \cdot L^{-1}}$
z	Position along the membrane	m
α	Purity	Dimensionless
δ	Ratio of diafiltrate to solvent flux	Dimensionless
δ^*	Critical ratio of diafiltrate to solvent flux	Dimensionless

Superscripts

Symbol	Meaning
R	Rectifying section
S	Stripping section

Subscripts

Symbol	Meaning
D	Diafiltrate
F	Feed
i	Solute i
j	Solute j
n	Stage number
P	Permeate
R	Retentate

s	Solute
w	Solvent
0	Inlet, Stage 0
1	Stage 1
2	Stage 2
3	Inlet, Stage 3

Supporting Information

Additional figures include: schematic of the experimental apparatus, calibration curves for the conductivity sensor, a sensitivity analysis of the retentate concentration predictions, semi-continuous retentate concentration versus feed volume data, a comparison of the retentate concentration measured experimentally and calculated from mass balances, predicted and experimental permeate concentration versus feed volume data, solute purity as a function of D/F for $S_i = 0.95$ and $S_j = 0.05$ systems, plots of solute recovery and purity as a function of D/F for $S_i = 0.8$ and $S_j = 0.2$ systems, contour maps of solute recovery and purity the stripping and rectifying sections as a function of solvent recovery. Additional equations include governing mass balances for a single stage system, additional derivations of the single stage concentration profile and solute recovery expressions, and solute balances and concentration profiles used to develop the matrix description of multistage stripping and rectifying sections. The Supporting Information is available free of charge on the ACS Publication website.

Acknowledgements

This work was made possible with support from the National Science Foundation (NSF) through the Advanced Manufacturing Program (Award Number: 1932206), and we appreciatively acknowledge this support. This work was partially supported by the NSF through the CAREER Program (Award Number: CBET-1941596). We would like to thank the Center for Environmental Science and Technology at the University of Notre Dame (CEST) portions of this research was

performed with instruments at this facility. C.P.K. gratefully acknowledges support for this project from the Vincent P. Slatt Fellowship for Undergraduate Research in Energy Systems and Processes, administered by the Center for Sustainable Energy at Notre Dame

References

(1) Sujanani, R.; Landsman, M. R.; Jiao, S.; Moon, J. D.; Shell, M. S.; Lawler, D. F.; Katz, L. E.; Freeman, B. D. Designing Solute-Tailored Selectivity in Membranes: Perspectives for Water Reuse and Resource Recovery. *ACS Macro Lett.* **2020**, *9* (11), 1709–1717. https://doi.org/10.1021/acsmacrolett.0c00710.

(2) Epsztein, R.; DuChanois, R. M.; Ritt, C. L.; Noy, A.; Elimelech, M. Towards Single-Species Selectivity of Membranes with Subnanometre Pores. *Nat. Nanotechnol.* **2020**, *15* (6), 426–436. https://doi.org/10.1038/s41565-020-0713-6.

(3) Werber, J. R.; Deshmukh, A.; Elimelech, M. The Critical Need for Increased Selectivity, Not Increased Water Permeability, for Desalination Membranes. *Environ. Sci. Technol. Lett.* **2016**, *3* (4), 112–120. https://doi.org/10.1021/acs.estlett.6b00050.

(4) Guest, J. S.; Skerlos, S. J.; Barnard, J. L.; Beck, M. B.; Daigger, G. T.; Hilger, H.; Jackson, S. J.; Karvazy, K.; Kelly, L.; Macpherson, L.; Mihelcic, J. R.; Pramanik, A.; Raskin, L.; Van Loosdrecht, M. C. M.; Yeh, D.; Love, N. G. A New Planning and Design Paradigm to Achieve Sustainable Resource Recovery from Wastewater. *Environ. Sci. Technol.* **2009**, *43* (16), 6126–6130. https://doi.org/10.1021/es9010515.

(5) Puyol, D.; Batstone, D. J.; Hülsen, T.; Astals, S.; Peces, M.; Krömer, J. O. Resource Recovery from Wastewater by Biological Technologies: Opportunities, Challenges, and Prospects. *Front. Microbiol.* **2017**, *0*. https://doi.org/10.3389/fmicb.2016.02106.

(6) Zhang, Y.; Almodovar-Arbelo, N. E.; Weidman, J. L.; Corti, D. S.; Boudouris, B. W.; Phillip, W. A. Fit-for-Purpose Block Polymer Membranes Molecularly Engineered for Water Treatment. *npj Clean Water* **2018**, *1* (1), 2. https://doi.org/10.1038/s41545-018-0002-1.

(7) Reck, B. K.; Graedel, T. E. Challenges in Metal Recycling. *Science* **2012**, *337* (6095), 690–695. https://doi.org/10.1126/science.1217501.

(8) Zeng, X.; Li, J.; Singh, N. Recycling of Spent Lithium-Ion Battery: A Critical Review. *Critical Reviews in Environmental Science and Technology* **2014**, *44* (10), 1129–1165. https://doi.org/10.1080/10643389.2013.763578.

(9) Li, C.; Ramasamy, D. L.; Sillanpää, M.; Repo, E. Separation and Concentration of Rare Earth Elements from Wastewater Using Electrodialysis Technology. *Separation and Purification Technology* **2021**, *254*, 117442. https://doi.org/10.1016/j.seppur.2020.117442.

(10) Rankin, W. J. *Minerals, Metals and Sustainability: Meeting Future Material Needs*; Csiro Publishing, 2011.

(11) Eckelman, M. J. Facility-Level Energy and Greenhouse Gas Life-Cycle Assessment of the Global Nickel Industry. *Resources, Conservation and Recycling* **2010**, *54* (4), 256–266. https://doi.org/10.1016/j.resconrec.2009.08.008.

(12) Rucker-Pezzini, J.; Arnold, L.; Hill-Byrne, K.; Sharp, T.; Avazhanskiy, M.; Forespring, C. Single Pass Diafiltration Integrated into a Fully Continuous MAb Purification Process. *Biotechnol Bioeng.* **2018**. https://doi.org/10.1002/bit.26608.

(13) Shao, J.; Zydney, A. L. Optimization of Ultrafiltration/Diafiltration Processes for Partially Bound Impurities. *Biotechnol Bioeng. 87* (3), 286–292. https://doi.org/10.1002/bit.20113.
(14) Zydney, A. L. New Developments in Membranes for Bioprocessing – A Review. *Journal of Membrane Science* **2021**, *620*, 118804. https://doi.org/10.1016/j.memsci.2020.118804.
(15) van Reis, R.; Zydney, A. Bioprocess Membrane Technology. *Journal of Membrane Science* **2007**, *297* (1), 16–50. https://doi.org/10.1016/j.memsci.2007.02.045.
(16) Hoffman, J. R.; Phillip, W. A. Dual-Functional Nanofiltration Membranes Exhibit Multifaceted Ion Rejection and Antifouling Performance. *ACS Appl. Mater. Interfaces* **2020**, *12* (17), 19944–19954. https://doi.org/10.1021/acsami.0c03075.
(17) Gao, F.; Hunter, A.; Qu, S.; Hoffman, J. R.; Gao, P.; Phillip, W. A. Interfacial Junctions Control Electrolyte Transport through Charge-Patterned Membranes. *ACS Nano* **2019**, *13* (7), 7655–7664. https://doi.org/10.1021/acsnano.9b00780.
(18) Guo, X.; Liu, D.; Han, T.; Huang, H.; Yang, Q.; Zhong, C. Preparation of Thin Film Nanocomposite Membranes with Surface Modified MOF for High Flux Organic Solvent Nanofiltration. *AIChE Journal* **2016**, *63* (4), 1303–1312.
(19) Qui, X.; Yu, H.; Karunakaran, M.; Pradeep, N.; Nunes, S.; Peinemann, K.-V. Selective Separation of Similarly Sized Proteins with Tunable Nanoporous Block Copolymer Membranes. *ACS Nano* **2012**, *7* (1), 768–776. https://doi.org/10.1021/nn305073e.
(20) Zhang, H.; Hou, X.; Zeng, L.; Yang, F.; Li, L.; Yan, D.; Tian, Y.; Jiang, L. Bioinspired Artificial Single Ion Pump. *J. Am. Chem. Soc.* **2013**, *135* (43), 16102–16110. https://doi.org/10.1021/ja4037669.
(21) Yang, Z.; Fang, W.; Wang, Z.; Zhang, R.; Zhu, Y.; Jin, J. Dual-Skin Layer Nanofiltration Membranes for Highly Selective Li+/Mg2+ Separation. *Journal of Membrane Science* **2021**, *620*, 118862. https://doi.org/10.1016/j.memsci.2020.118862.
(22) Wang, L.; Rehman, D.; Sun, P.-F.; Deshmukh, A.; Zhang, L.; Han, Q.; Yang, Z.; Wang, Z.; Park, H.-D.; Lienhard, J. H.; Tang, C. Y. Novel Positively Charged Metal-Coordinated Nanofiltration Membrane for Lithium Recovery. *ACS Appl. Mater. Interfaces* **2021**, *13* (14), 16906–16915. https://doi.org/10.1021/acsami.1c02252.
(23) Zhang, S.; Ou, R.; Ma, H.; Lu, J.; Banaszak Holl, M. M.; Wang, H. Thermally Regenerable Metal-Organic Framework with High Monovalent Metal Ion Selectivity. *Chemical Engineering Journal* **2021**, *405*, 127037. https://doi.org/10.1016/j.cej.2020.127037.
(24) National Academies of Sciences, E. *A Research Agenda for Transforming Separation Science*; 2019. https://doi.org/10.17226/25421.
(25) Eugene, E. A.; Phillip, W. A.; Dowling, A. W. Data Science-Enabled Molecular-to-Systems Engineering for Sustainable Water Treatment. *Current Opinion in Chemical Engineering* **2019**, *26*, 122–130. https://doi.org/10.1016/j.coche.2019.10.002.
(26) Konstantinov, K. B.; Cooney, C. L. White Paper on Continuous Bioprocessing May 20–21 2014 Continuous Manufacturing Symposium. *Journal of Pharmaceutical Sciences* **2015**, *104* (3), 813–820. https://doi.org/10.1002/jps.24268.
(27) Nambiar, A. M. K.; Li, Y.; Zydney, A. L. Countercurrent Staged Diafiltration for Formulation of High Value Proteins. *Biotechnology and Bioengineering 115* (1), 139–144. https://doi.org/10.1002/bit.26441.
(28) Jabra, M. G.; Yehl, C. J.; Zydney, A. L. Multistage Continuous Countercurrent Diafiltration for Formulation of Monoclonal Antibodies. *Biotechnology Progress* **2019**, *35* (4), e2810. https://doi.org/10.1002/btpr.2810.

(29) Siew, W. E.; Livingston, A. G.; Ates, C.; Merschaert, A. Continuous Solute Fractionation with Membrane Cascades – A High Productivity Alternative to Diafiltration. *Separation and Purification Technology* **2013**, *102*, 1–14. https://doi.org/10.1016/j.seppur.2012.09.017.
(30) Barker, P. E.; Till, A. Using Multistage Techniques to Improve Diafiltration Fractionation Efficiency. *Journal of Membrane Science* **1992**, *72* (1), 1–11. https://doi.org/10.1016/0376-7388(92)80051-K.
(31) Tan, R.; Hezel, F.; Franzreb, M. Continuous Single Pass Diafiltration with Alternating Permeate Flow Direction for High Efficiency Buffer Exchange. *Journal of Membrane Science* **2021**, *619*, 118695. https://doi.org/10.1016/j.memsci.2020.118695.
(32) Mehta, A.; Zydney, A. L. Permeability and Selectivity Analysis for Ultrafiltration Membranes. *Journal of Membrane Science* **2005**, *249* (1), 245–249. https://doi.org/10.1016/j.memsci.2004.09.040.
(33) Ouimet, J. A.; Liu, X.; Brown, D. J.; Eugene, E. A.; Popps, T.; Muetzel, Z. W.; Dowling, A. W.; Phillip, W. A. DATA: Diafiltration Apparatus for High-Throughput Analysis. *Journal of Membrane Science* **2021**, 119743. https://doi.org/10.1016/j.memsci.2021.119743.
(34) Ghosh, R.; Chen, G.; Roshankhah, R.; Umatheva, U.; Gatt, P. A Z2 Laterally-Fed Membrane Chromatography Device for Fast High-Resolution Purification of Biopharmaceuticals. *Journal of Chromatography A* **2020**, *1629*, 461453. https://doi.org/10.1016/j.chroma.2020.461453.
(35) Ghosh, R.; Madadkar, P.; Wu, Q. On the Workings of Laterally-Fed Membrane Chromatography. *Journal of Membrane Science* **2016**, *516*, 26–32. https://doi.org/10.1016/j.memsci.2016.05.064.
(36) Madadkar, P.; Wu, Q.; Ghosh, R. A Laterally-Fed Membrane Chromatography Module. *Journal of Membrane Science* **2015**, *487*, 173–179. https://doi.org/10.1016/j.memsci.2015.03.056.
(37) Sadavarte, R.; Madadkar, P.; Filipe, C. D.; Ghosh, R. Rapid Preparative Separation of Monoclonal Antibody Charge Variants Using Laterally-Fed Membrane Chromatography. *Journal of Chromatography B* **2018**, *1073*, 27–33. https://doi.org/10.1016/j.jchromb.2017.12.003.
(38) Tan, R.; Franzreb, M. Continuous Ultrafiltration/Diafiltration Using a 3D-Printed Two Membrane Single Pass Module. *Biotechnology and Bioengineering* **2020**, *117* (3), 654–661. https://doi.org/10.1002/bit.27233.
(39) Opare, E. O.; Struhs, E.; Mirkouei, A. A Comparative State-of-Technology Review and Future Directions for Rare Earth Element Separation. *Renewable and Sustainable Energy Reviews* **2021**, *143*, 110917. https://doi.org/10.1016/j.rser.2021.110917.
(40) Huang, B.; Pan, Z.; Su, X.; An, L. Recycling of Lithium-Ion Batteries: Recent Advances and Perspectives. *Journal of Power Sources* **2018**, *399*, 274–286. https://doi.org/10.1016/j.jpowsour.2018.07.116.

For Table of Contents Use Only

Staged Diafiltration Cascades Provide Opportunities to Execute Highly Selective Separations

Cara P. Kilmartin, Jonathan Aubuchon Ouimet, Alexander W. Dowling, and William A. Phillip

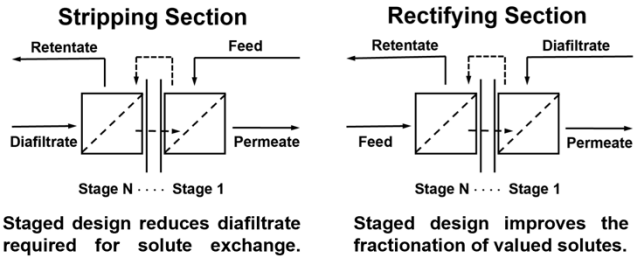

Biosketch

Staged Diafiltration Cascades Provide Opportunities to Execute Highly Selective Separations

Cara P. Kilmartin, Jonathan Aubuchon Ouimet, Alexander W. Dowling, and William A. Phillip

Cara P. Kilmartin was born in Wilton, CT and will be receiving her Bachelor of Science in Chemical Engineering from the University of Notre Dame in 2022. She began her research on modeling and experimentally characterizing diafiltration processes in 2020. In 2021, she was awarded the Vincent P. Slatt Fellowship for Undergraduate Research in Energy Systems and Processes to support her interest in energy-efficient and sustainable separation processes.

Jonathan Aubuchon Ouimet received his Bachelor's Degree in Chemical Engineering from Miami University (OH) in 2019. Following graduation, Jonathan began his doctoral studies in Chemical and Biomolecular Engineering at the University of Notre Dame. Jonathan is a recipient of the National Science Foundation Graduate Research Fellowships Program Honorable Mention. His doctoral research aims to understand the transport phenomena that governs molecular separations in order to mimic the facilitated transport mechanisms of biological ion pumps.

Dr. Alexander Dowling is an Assistant Professor of Chemical and Biomolecular Engineering at the University of Notre Dame. He earned his B.S.E. in Chemical Engineering from the University of Michigan – Ann Arbor in 2010; and completed his Ph.D. in Chemical Engineering at Carnegie Mellon University in 2015. Before joining Notre Dame in 2017, he was a postdoctoral fellow at the University of Wisconsin – Madison. Professor Dowling and his group develop process systems

engineering and data science methods to enable molecular-to-systems optimization of energy and environmental technologies. Dr. Dowling and his team have been recognized with the National Science Foundation CAREER award and an R&D 100 award.

Dr. William Phillip is the Rooney Family Collegiate Associate Professor of Engineering in the Department of Chemical and Biomolecular Engineering at the University of Notre Dame. He received his B.S. from the University of Notre Dame in 2004; and completed his Ph.D. under the guidance of Prof. Ed Cussler at the University of Minnesota in 2009. Following his Ph.D., Dr. Phillip completed a postdoctoral appointment with Prof. Menachem Elimelech at Yale University. His research group seeks to develop energy-efficient separation processes at the water-energy nexus through the design and fabrication of membranes that provide more precise control over mass transfer. Dr. Phillip and his team have been recognized with the FRI/John G. Kunesh Award from the American Institute of Chemical Engineers, the Duncan and Suzanne Mellichamp Lectureship at Purdue University, the Rev. Edmund P. Joyce, C.S.C., Award for Excellence in Undergraduate Teaching, and the College of Engineering Outstanding Teaching Award.